Phys. Status Solidi B **246**, No. 9, 2033–2044 (2009) / **DOI** 10.1002/pssb.200982034

physica status solidi b
www.pss-b.com
basic solid state physics

On rotating rigid parallelograms and their potential for exhibiting auxetic behaviour

Daphne Attard, Elaine Manicaro, and Joseph N. Grima*

Department of Chemistry, Faculty of Science, University of Malta, Msida MSD 2080, Malta

Received 30 April 2009, revised 25 May 2009, accepted 25 May 2009
Published online 12 August 2009

PACS 62.20.dj, 81.05.Zx

* Corresponding author: e-mail joseph.grima@um.edu.mt, Phone: +356 2340 2274, Fax: +356 2540 1091
Internet: www.auxetic.info

Auxetic systems have the anomalous property of becoming wider when uniaxially stretched, *i.e.* exhibit a negative Poisson's ratio. One of the mechanisms which can give rise to this property is based on rotating rigid units, in particular 2D rigid polygons which are connected together at their corners through hinges and rotate relative to each other when uniaxially stretched. This work extends earlier preliminary work on connected rigid parallelograms and presents expressions for the mechanical properties for all the types of planar systems that can be constructed from rigid parallelograms of equal size connected at their vertices through flexible hinges. In particular, we derive and discuss the mechanical properties for the Type Iα, Iβ and IIβ rotating parallelograms which were not previously analysed and compare them with the properties of the Type IIα systems. We show that despite being rather similar to each other, the different types of 'rotating parallelograms' have very different mechanical properties and different abilities to exhibit auxetic behaviour.

1 Introduction The behaviour of a material when subjected to external stresses is characterized by its mechanical properties. In particular, the Poisson's ratio ν_{ij} in the $Ox_i - Ox_j$ plane describes how the dimensions of the system change as it is uniaxially loaded along the Ox_i direction and is mathematically defined as the negative of the ratio of the strain ε_j along the lateral direction (Ox_j) and the strain ε_i along the loading direction Ox_i, *i.e.*

$$\nu_{ij} = -\frac{\varepsilon_j}{\varepsilon_i}. \tag{1}$$

Note that for conventional materials which become thinner when stretched, the Poisson's ratio assumes positive values, whereas for auxetic materials which expand laterally when stretched, it assumes negative values. Materials which possess auxeticity have been found to have enhanced qualities when compared to conventional materials, including a better indentation resistance [1–3], an enhanced ability to form doubly curved surfaces [1, 4–6] and improved acoustic properties [7–9].

The ability to exhibit such a counter-intuitive behaviour is often linked to particular geometrical features of the system and also on how it deforms [1]. In past decades there was significant progress in this area [10–56] and among the first systems studied for their potential to exhibit auxetic behaviour are systems based on rigid 'free' molecules and hard-body sytems [10–15], self-avoiding fixed-connectivity membranes [16], re-entrant [4, 17–20, 35] and chiral [21–22] honeycombs deforming through flexure or hinging, and rotating rigid or semi-rigid 2D [23–30] and 3D units [31–34]. In these systems, auxeticity has been found to be scale independent, *i.e.* the same mechanism can operate at any length scale. In fact, such mechanisms have been used to design potentially auxetic hypothetical systems [20, 36–42] and to explain auxeticity on a microlevel in cellular materials such as foams [5, 43–46] and microstructured polymers [48–50] as well as at the nanolevel in several molecular-level auxetics, such as silicates [31–34, 51–52], metals [53] and liquid crystalline polymers [54–55]. In particular, 2D rigid/semi-rigid rotating unit mechanisms have been found particularly useful in explaining the auxeticity exhibited by various zeolitic frameworks [26, 30, 56] and also in silicates like cristobalite [31–34, 51–52].

In this work we attempt to expand existing knowledge about this class of systems by considering networks based on rigid parallelograms which can be considered as a more generalized form of squares, rhombi and rectangles.

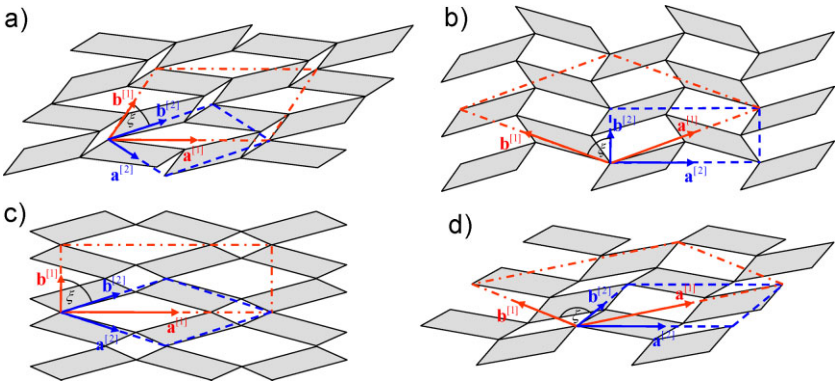

Figure 1 (online colour at: www.pss-b.com) The four possible networks that can be constructed from parallelograms: the space filling Type Iα (a) and Type IIα (b) and non-space filling Type Iβ (c) and Type IIβ (d) rotating parallelograms systems. The unit cells for Orientation 1 (dash-dot-dash) and Orientation 2 (dash) are also shown for each of the networks.

Although the different networks that can be possibly constructed from rigid parallelograms have already been shown in [28], only the mechanical properties for one of the four networks have been derived (those for the Type IIα system). In view of this, here we derive the full 3×3 stiffness matrices for the three rotating parallelograms systems which have not been studied so far, *i.e.* the Type Iα, Type Iβ and Type IIβ networks and discuss their potential as auxetic systems.

2 Rotating rigid parallelograms Like squares, rectangles, rhombi and triangles, parallelograms can be connected together to form planar tessellations. Their geometry, characterized by two sets of parallel sides with opposite angles that are congruent, allows, as described in [28], for different types of connections which can have:

(i) *either* an α*-type* of connection in which case adjacent parallelograms are connected together such that at each hinge, one of the smaller angles of a parallelogram is connected to one of the larger angles of an adjacent parallelogram[1] *or* a β*-type* connection where adjacent parallelograms have like angles connected together and
(ii) *either* a *I-type* connection where parallelograms have sides of the same length connected together giving rise to two different rhombic pore sizes within the network *or* a *II-type* connection where the sides of adjacent parallelograms forming a loop are of an alternating length so that the resulting pores all have the same length dimensions and are parallelograms in shape.

This results in four different combinations – the *Type I*α, *Type II*α, *Type I*β and *Type II*β rotating parallelograms, of which only the Type Iα and Type IIα are space filling, as illustrated in Fig. 1.

Similar to other systems [57, 29], these networks can be easily described by either of two unit cells having different orientations which we refer to as 'Orientation 1' and 'Orientation 2' (see Fig. 1). In all cases, 'Orientation 1' is the larger of the unit cells and contains four whole parallelograms, while that in 'Orientation 2' contains only two. Furthermore, the two orientations can be geometrically related since one of the diagonals of the unit cell in 'Orientation 2' is also the cell vector $\boldsymbol{a}$ for the unit cell in 'Orientation 1', from which it follows that the angle ξ which relates the two orientations is in fact the angle between the diagonal and cell vector $\boldsymbol{b}$ of the unit cell in 'Orientation 1'. We note that all analytical models for the similar systems considered so far have been derived in one of these orientations: the Type I 'rotating rectangles' were derived in Orientation 1, the Type IIα parallelograms/rhombi were derived in Orientation 2 whilst the 'rotating squares', Type II 'rotating rectangles' and Type β 'rotating rhombi' were derived for any orientation given that they are isotropic in-plane [23, 25, 29]. In view of this, in an attempt to enable a comparison between the rotating parallelograms and the more specific cases of 'rotating rectangles/rhombi or squares', we shall derive the mechanical properties of the Type Iα and Type Iβ rotating parallelograms (which are anisotropic) in Orientation 1 to enable a quick comparison with the Type I rotating rectangles and in Orientation 2 (given in Appendix A) to enable a comparison with the properties of rhombi[2]. We will also be deriving the properties of the Type IIβ rotating parallelograms in Orientation 2 although in this case the properties derived will be applicable in any orientation since, as we will show, the system is isotropic in-plane[3].

Throughout this work we will be adopting the convention of aligning the unit cell vector $\boldsymbol{b}$ parallel to the Ox_2 direction

[1] Note that all the parallelograms making up any one of the systems considered here have the same dimensions so that for Type α systems, the internal angles of adjacent parallelograms at each hinge are complementary.

[2] Note that the equations for the properties in any orientation may be derived from any single orientation using standard axis transformation techniques [59]. In particular, the expressions for the mechanical properties of the systems in Orientation 2 may be obtained directly from those in Orientation 1 using standard axis transformation technique, and *vice versa*. Nevertheless, due to the algebraic complexity of the expressions involved, only the simplified expressions in these two main orientations are presented here.

[3] The properties of the Type IIα systems have already been derived elsewhere.

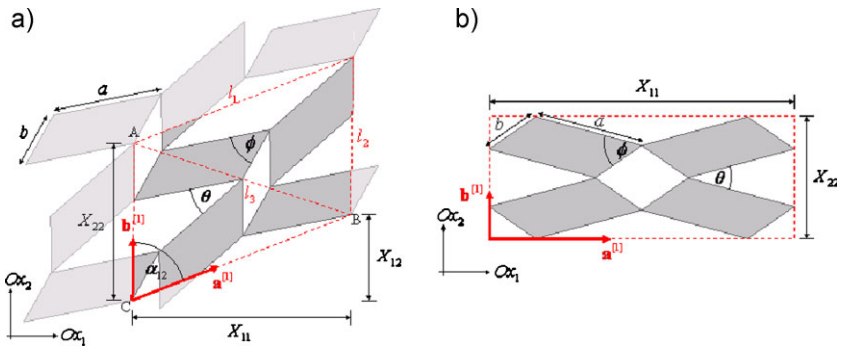

Figure 2 (online colour at: www.pss-b.com) Geometrical parameters describing the unit cell for (a) Type Iα and (b) Type Iβ rotating parallelograms in Orientation 1.

while $\boldsymbol{a}$ lies in the $Ox_1 - Ox_2$ plane and points in the direction dictated by the dimensions of the parallelograms (the sides a and b and the internal angle ϕ) and the angle θ between them (the degree of openness) so that the unit cell of each network can be most generally described by the unit cell vectors $\boldsymbol{a} = (X_{11},\ X_{12})$ and $\boldsymbol{b} = (0,\ X_{22})$, lying at angle α_{12} away from each other. Assuming that the parallelograms are perfectly rigid, the changes in shape and size of the unit cell occurring during deformation are a function of the single variable θ.

3 On-axis mechanical properties

3.1 Type Iα rotating parallelograms in orientation 1 Referring to Fig. 2a, Type Iα networks are described by a parallelogramic unit cell for which:

$$X_{11} = \frac{A}{l_2}, \tag{2}$$

$$X_{22} = l_2, \tag{3}$$

$$X_{12} = \sqrt{l_1^2 - \frac{4A^2}{l_2^2}} \tag{4}$$

$$\alpha_{12} = \cos^{-1}\left(\frac{l_1^2 + l_2^2 - l_3^2}{2l_1 l_2}\right), \tag{5}$$

where α_{12} is the internal angle of the unit cell and l_1 and l_2 are its side lengths given by

$$l_1 = 2\sqrt{a^2\cos^2\left(\frac{\theta}{2}\right) + b^2\sin^2\left(\frac{\theta}{2}\right) + ab\sin(\theta)\sin(\phi)}, \tag{6}$$

$$l_2 = 2\sqrt{a^2\sin^2\left(\frac{\theta}{2}\right) + b^2\cos^2\left(\frac{\theta}{2}\right) + ab\sin(\theta)\sin(\phi)}, \tag{7}$$

and A is the area of the unit cell which can be found using Heron's formula *i.e.* $A = 2\sqrt{s(s-l_1)(s-l_2)(s-l_3)}$ where s is the half-perimeter of triangle ABC and l_3 (the diagonal of the unit cell opposite α_{12}, see Fig. 2a), given respectively by

$$s = \frac{l_1 + l_2 + l_3}{2}, \tag{8}$$

$$l_3 = 2\sqrt{a^2 + b^2 - 2ab\cos(\theta + \phi)}. \tag{9}$$

It is important to note that the fact that α_{12} is dependent on θ suggests that the unit cell shears upon deformation so that all the nine coefficients in the 3×3 stiffness matrix may have a non-zero value, *i.e.*

$$\mathbf{S} = \begin{pmatrix} s_{11} & s_{12} & s_{13} \\ s_{21} & s_{22} & s_{23} \\ s_{31} & s_{32} & s_{33} \end{pmatrix} = \begin{pmatrix} \frac{1}{E_1} & \frac{-\nu_{21}}{E_2} & \frac{\eta_{31}}{G_{12}} \\ \frac{-\nu_{12}}{E_1} & \frac{1}{E_2} & \frac{\eta_{32}}{G_{12}} \\ \frac{\eta_{13}}{E_1} & \frac{\eta_{23}}{E_2} & \frac{1}{G_{12}} \end{pmatrix} \tag{10}$$

meaning that in order to properly analyse the system, including its off-axis mechanical properties, it is necessary to derive the Poisson's ratios, ν_{ij}, Young's moduli, E_i, shear modulus, G_{12} and shear coupling coefficients, η_{ij}.

3.1.1 Poisson's ratios The strains along the Ox_1 and Ox_2 directions can be obtained after substituting for A in Eq. (2) and expressing the resultant equation in terms of the infinitesimal change in the angle $\mathrm{d}\theta$ as

$$\varepsilon_1 = \frac{\mathrm{d}X_{11}}{X_{11}} = \frac{1}{X_{11}}\left[\left(\frac{\partial X_{11}}{\partial l_1}\right)_{l_2,l_3}\left(\frac{\mathrm{d}l_1}{\mathrm{d}\theta}\right) + \left(\frac{\partial X_{11}}{\partial l_2}\right)_{l_1,l_3}\left(\frac{\mathrm{d}l_2}{\mathrm{d}\theta}\right) + \left(\frac{\partial X_{11}}{\partial l_3}\right)_{l_1,l_2}\left(\frac{\mathrm{d}l_3}{\mathrm{d}\theta}\right)\right]\mathrm{d}\theta, \tag{11}$$

$$\varepsilon_2 = \frac{\mathrm{d}X_{22}}{X_{22}} = \frac{1}{X_{22}}\left(\frac{\mathrm{d}l_2}{\mathrm{d}\theta}\right)\mathrm{d}\theta, \tag{12}$$

so that on differentiating Eqs. (6),(7) and (9) with respect to θ and substituting into Eqs. (11) and (12), the Poisson's ratio for loading in the Ox_2 direction can, after simplifying,

be written as

$$\nu_{21} = (\nu_{12})^{-1} = -\frac{\varepsilon_1}{\varepsilon_2} = -\frac{\left(a^2-b^2\right)\left(l_2^2l_1^2-l_2^4-A^2\right)\sin(\theta)+2abl_2^2\left(l_2^2+l_1^2-l_3^2\right)\sin(\theta+\phi)+2ab\cos(\theta)\sin(\phi)\left(l_3^2l_2^2-A^2\right)}{\left[\left(a^2-b^2\right)\sin(\theta)+2ab\cos(\theta)\sin(\phi)\right]A^2} \tag{13}$$

3.1.2 Young's moduli The Young's moduli can be found using an energy approach. The work done at each hinge in changing the angle θ by $\mathrm{d}\theta$ is given by:

$$W = \frac{1}{2}K_h\mathrm{d}\theta^2. \tag{14}$$

Since there are eight hinges in each unit cell, the total strain energy U stored per unit volume V is given by:

$$U = \frac{4K_h\mathrm{d}\theta^2}{V} = \frac{1}{2}E_i\varepsilon_i^2, \tag{15}$$

where E_i is the Young's modulus of the network along the Ox_i direction and $V = X_{11}X_{22}z$, with z being the out-of-plane thickness of the parallelograms so that using Eqs. (2), (3), (11) and (12), the Young's moduli can be expressed by

$$E_1 = \frac{8K_hl_2^4A^3}{z}\left[\left(a^2-b^2\right)\left(l_1^2l_2^2-l_2^4-A^2\right)\sin(\theta)+2ab\cos(\theta)\sin(\phi)\left(l_2^2l_3^2-A^2\right)+2abl_2^2\left(l_1^2+l_2^2-l_3^2\right)\sin(\theta+\phi)\right]^{-2}, \tag{16}$$

$$E_2 = \frac{8K_hl_2^4}{zA\left[\left(a^2-b^2\right)\sin(\theta)+2ab\cos(\theta)\sin(\phi)\right]^2}. \tag{17}$$

3.1.3 Shear modulus As previously stated, the unit cell for this network also shears, *i.e.* the internal angle α_{12} of the unit cell does not remain constant during deformation, resulting in a shear strain γ. To derive the shear modulus we first define the shear strain in terms of $\mathrm{d}\theta$ as follows [36, 58]:

$$\gamma = \frac{1}{X_{11}}\left[\mathrm{d}X_{12}-\left(\frac{X_{12}}{X_{22}}\right)\mathrm{d}X_{22}\right] = \frac{1}{X_{11}}\left(\cos(\alpha_{12})\left(\frac{\mathrm{d}l_1}{\mathrm{d}\theta}\right)-l_1\sin(\alpha_{12})\left(\frac{\mathrm{d}\alpha_{12}}{\mathrm{d}\theta}\right)-\frac{X_{12}}{l_2}\left(\frac{\mathrm{d}l_2}{\mathrm{d}\theta}\right)\right)\mathrm{d}\theta, \tag{18}$$

where

$$X_{12} = l_1\cos(\alpha_{12}) \text{ and } \sin(\alpha_{12}) = \sqrt{1-\left(\frac{X_{12}}{l_1}\right)^2} = \frac{X_{11}}{l_1}, \tag{19}$$

so that using Eqs. (2) and (4–6) and simplifying, the shear strain can be rewritten as

$$\gamma = \frac{\left(a^2-b^2\right)\sin(\theta)\left(l_3^2-l_2^2-l_1^2\right)+2ab\cos(\theta)\sin(\phi)\left(l_3^2+l_2^2-l_1^2\right)-4abl_2^2\sin(\theta+\phi)}{Al_2^2}. \tag{20}$$

Having derived the shear strain γ in terms of $\mathrm{d}\theta$ the shear modulus may be obtained using an energy conservation approach. In particular, the shear modulus G_{12} can be related to γ and the total energy U stored in the system, through the following equation:

$$U = \frac{2K_h\mathrm{d}\theta^2}{V} = \frac{1}{2}G_{12}\gamma^2, \tag{21}$$

from which it follows that

$$G_{12} = \frac{8K_hl_2^4A}{z\left[\left(a^2-b^2\right)\left(l_3^2-l_2^2-l_1^2\right)\sin(\theta)+2ab\left(l_3^2+l_2^2-l_1^2\right)\cos(\theta)\sin(\phi)-4abl_2^2\sin(\theta+\phi)\right]^2}. \tag{22}$$

Using the expressions obtained for the normal strains ε_i and the shear strains γ, the shear coupling coefficients η_{13}, η_{31}, η_{23} and η_{32} can also be found since:

$$\eta_{i3} = \frac{\gamma}{\varepsilon_i} \text{ and } \eta_{3i} = \frac{\varepsilon_i}{\gamma}\ (i = 1, 2). \tag{23}$$

3.2 Type Iβ rotating parallelograms in orientation 1 For Type Iβ networks, it is evident from Fig. 2b that $\alpha_{12} = \pi/2$ *i.e.* the unit cell in this orientation has a rectangular shape and does not shear. In this case, the unit cell is described by the unit cell vectors $\boldsymbol{a} = (X_{11}, 0)$ and $\boldsymbol{b} = (0, X_{22})$ where referring to Fig. 2b:

$$X_{11} = 2\left[a\cos\left(\frac{\theta}{2}\right)+b\cos\left(\phi-\frac{\theta}{2}\right)\right], \tag{24}$$

$$X_{22} = 2\left[a\sin\left(\frac{\theta}{2}\right)+b\sin\left(\phi-\frac{\theta}{2}\right)\right]. \tag{25}$$

For such systems, the stiffness matrix describing the on-axis mechanical properties has only four non-zero

coefficients and is given by:

$$\mathbf{S} = \begin{pmatrix} s_{11} & s_{12} & s_{13} \\ s_{21} & s_{22} & s_{23} \\ s_{31} & s_{32} & s_{33} \end{pmatrix} = \begin{pmatrix} \frac{1}{E_1} & \frac{-\nu_{21}}{E_2} & 0 \\ \frac{-\nu_{12}}{E_1} & \frac{1}{E_2} & 0 \\ 0 & 0 & 0 \end{pmatrix} \tag{26}$$

i.e. the mechanical properties of these systems are totally describable by the on-axis Poisson's ratio and Young's moduli.

3.2.1 Poisson's ratios The strains along the Ox_i directions may be defined in terms of $\mathrm{d}\theta$ and are given by

$$\varepsilon_i = \frac{\mathrm{d}X_i}{X_i} = \frac{1}{X_i}\left(\frac{\mathrm{d}X_i}{\mathrm{d}\theta}\right)\mathrm{d}\theta, \tag{27}$$

so that on differentiating Eqs (24) and (25) with respect to θ, the strains can be rewritten as:

$$\varepsilon_1 = -\frac{a\sin\left(\frac{\theta}{2}\right) - b\sin\left(\phi - \frac{\theta}{2}\right)}{2\left[a\sin\left(\frac{\theta}{2}\right) + b\sin\left(\phi - \frac{\theta}{2}\right)\right]}\mathrm{d}\theta, \tag{28}$$

$$\varepsilon_2 = \frac{a\cos\left(\frac{\theta}{2}\right) - b\cos\left(\phi - \frac{\theta}{2}\right)}{2\left[a\sin\left(\frac{\theta}{2}\right) + b\sin\left(\phi - \frac{\theta}{2}\right)\right]}\mathrm{d}\theta, \tag{29}$$

and on substituting in Eq. (1) and simplifying, the Poisson's ratio is given by:

$$\nu_{21} = (\nu_{12})^{-1} = \frac{a^2\sin^2\left(\frac{\theta}{2}\right) - b^2\sin^2\left(\phi - \frac{\theta}{2}\right)}{a^2\cos^2\left(\frac{\theta}{2}\right) - b^2\cos^2\left(\phi - \frac{\theta}{2}\right)}. \tag{30}$$

3.2.2 Young's moduli Using the energy approach already outlined for the Type Iα systems, the Young's moduli are found to be given by the following equations:

$$E_1 = \frac{8K_h\left[a\cos\left(\frac{\theta}{2}\right) + b\cos\left(\phi - \frac{\theta}{2}\right)\right]}{z\left[a\sin\left(\frac{\theta}{2}\right) + b\sin\left(\phi - \frac{\theta}{2}\right)\right]\left[a\sin\left(\frac{\theta}{2}\right) - b\sin\left(\phi - \frac{\theta}{2}\right)\right]^2}, \tag{31}$$

$$E_2 = \frac{8K_h\left[a\sin\left(\frac{\theta}{2}\right) + b\sin\left(\phi - \frac{\theta}{2}\right)\right]}{z\left[a\cos\left(\frac{\theta}{2}\right) + b\cos\left(\phi - \frac{\theta}{2}\right)\right]\left[a\cos\left(\frac{\theta}{2}\right) - b\cos\left(\phi - \frac{\theta}{2}\right)\right]^2}. \tag{32}$$

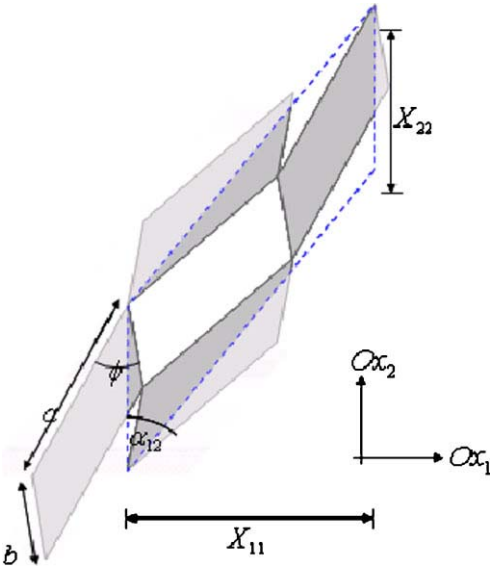

Figure 3 (online colour at: www.pss-b.com) Geometrical parameters describing the unit cell for Type IIβ rotating parallelograms in orientation 2.

3.3 Type IIβ rotating parallelograms in orientation 2 The unit cell in orientation 2 for Type IIβ configuration is shown in Fig. 3. In this case the unit cell is described by the unit cell vectors $\boldsymbol{a} = (X_{11}, X_{12})$ and $\boldsymbol{b} = (0, X_{22})$ lying at an angle $\alpha_{12} = \phi$ to each other so that:

$$X_{11} = 2a\cos\left(\frac{\theta - \phi}{2}\right)\sin\phi, \tag{33}$$

$$X_{22} = 2b\cos\left(\frac{\theta - \phi}{2}\right), \tag{34}$$

$$X_{12} = 2a\cos\left(\frac{\theta - \phi}{2}\right)\cos\phi. \tag{35}$$

The fact that the relative orientation of the cell vectors is only dependent on ϕ suggests that in this orientation, the network does not shear *i.e.* has an infinite shear modulus so that the compliance matrix is given by Eq. (26). Thus, as for the Type Iβ systems, to fully describe the mechanical properties of the system it is sufficient to derive analytical models for the Poisson's ratios and Young's moduli.

3.3.1 Poisson's ratio From Eqs (33) and (34), it can be found that the strains in both Ox_i directions are given by

$$\varepsilon_i = \frac{\mathrm{d}X_i}{X_i} = \frac{1}{X_i}\left(\frac{\mathrm{d}X_i}{\mathrm{d}\theta}\right)\mathrm{d}\theta = -\frac{1}{2}\tan\left(\frac{\theta - \phi}{2}\right)\mathrm{d}\theta, \tag{36}$$

i.e.

$$\nu_{21} = (\nu_{12})^{-1} = -\frac{\varepsilon_1}{\varepsilon_2} = -1 \tag{37}$$

i.e. the Poisson's ratio is -1 irrespective of a, b, θ and ϕ.

3.3.2 Young's moduli Using an energy approach, and taking into account that the unit cell contains four hinges, the Young's modulus can be related to the strain energy as follows:

$$U = \frac{4K_h \mathrm{d}\theta^2}{2V} = \frac{1}{2} E_i \varepsilon_i^2, \tag{38}$$

where $\frac{1}{2}K_h \mathrm{d}\theta^2$ is the work done at each hinge and V is the volume of the unit cell given by $X_{11}X_{22}z$ with z being the out-of-plane thickness of the parallelograms, so that the Young's modulus can be given by:

$$E_i = \frac{4K_h}{zab\sin\phi \sin\left(\dfrac{\theta-\phi}{2}\right)^2}. \tag{39}$$

4 Off-axis mechanical properties The off-axis mechanical properties of these systems can be computed using standard axis transformation techniques [59] and it can be shown that the Type Iα, Type Iβ and Type IIα are highly anisotropic. In contrast to this, standard axes transformation techniques [59] suggest that the Type IIβ system is isotropic in-plane, *i.e.* the Poisson's ratio is always -1 irrespective of the direction of loading and the full compliance matrix is always given by:

$$\mathbf{S} = \begin{pmatrix} s_{11} & s_{12} & 0 \\ s_{21} & s_{22} & 0 \\ 0 & 0 & 0 \end{pmatrix} = \frac{1}{E}\begin{pmatrix} 1 & 1 & 0 \\ 1 & 1 & 0 \\ 0 & 0 & 0 \end{pmatrix} = \frac{zab\sin\phi \sin\left(\dfrac{\theta-\phi}{2}\right)^2}{4K_h}\begin{pmatrix} 1 & 1 & 0 \\ 1 & 1 & 0 \\ 0 & 0 & 0 \end{pmatrix}. \tag{40}$$

5 Results and discussion The equations derived above clearly show that the Type IIβ parallelograms exhibit a constant Poisson's ratio of -1 irrespective of the shape and size of the parallelograms, the degree of openness of the system and the direction of loading. This is very different from what is observed in the Type IIα systems (discussed in [28]) and the Type Iα and Iβ systems as illustrated in the plots in Fig. 4 which show the variation of the Poisson's ratio with the angle θ for different Type Iα and Type Iβ networks in Orientation 1 for loading in the Ox_2 direction.

The plots in Fig. 4 clearly highlight that the sign and magnitude of the on-axis Poisson's ratios for these Type I networks in Orientation 1 are dependent on the shape of the parallelograms, in particular on the aspect ratio a/b and on its internal angle ϕ, and are also highly dependent on the angle between the parallelograms (which in turn suggests that the properties of these systems are highly strain dependent). For these systems, if one re-writes the expression for the on-axis Poisson's ratio in Orientation 1 for the particular case when the systems are fully closed (*i.e.* at $\theta = 0^\circ$), one finds that for the Type Iα systems, the Poison's ratio at $\theta = 0^\circ$ has a value given by:

$$\nu_{21}^{\theta=0} = \left(\nu_{12}^{\theta=0}\right)^{-1} = -\frac{l_2^4 + l_1^2 l_2^2 - A^2}{A^2}, \tag{41}$$

for which it can be easily shown that $A < l_1 l_2$, meaning that the Poisson's ratio corresponding to the fully closed configuration for Type Iα parallelograms is always negative, *i.e.* they are always initially auxetic when stretched from their fully closed configuration. On the other hand, Type Iβ networks can have both a negative as well as a positive Poisson's ratio when $\theta = 0^\circ$ which is given by the expression:

$$\nu_{21}^{\theta=0} = \left(\nu_{12}^{\theta=0}\right)^{-1} = -\frac{b^2 \sin^2(\phi)}{a^2 - b^2\cos^2(\phi)}, \tag{42}$$

where since $0 < \sin(\phi) < 1$, it follows that ν_{21} is positive if $a/b < \cos(\phi)$ and negative if $a/b > \cos(\phi)$, the latter of which implies that for any system having $a > b$, $\nu_{21}^{\theta=0}$ is negative irrespective of ϕ. In cases where $a/b = \cos(\phi)$, the Poisson's ratio tends to ∞ as $\theta \to 0^\circ$, assuming that no overlap of the parallelograms occurs, *i.e.* $\theta \geq 0^\circ$. Thus, the initial behaviour of Type Iβ systems is highly dependent on the relative magnitude of the aspect ratio of the parallelograms and its internal angle.

It is also evident from Fig. 4 that the on-axis Poisson's ratio undergoes transitions from negative to positive values or *vice versa*. Such transitions can occur either continuously with a gradual change in the Poisson's ratio, passing smoothly through zero or discontinuously where changes occur from a positive to a negative extreme (or *vice versa*) over the smallest of changes in θ. From a mathematical point of view such instances arise when either the numerator or the denominator in the expressions describing the Poisson's ratio equates to zero.

In the case of Type Iα parallelograms, continuous transitions for ν_{21} occur when[4]:

$$\left(a^2 - b^2\right)\left(l_2^2 l_1^2 - l_2^4 - A^2\right)\sin(\theta) + 2abl_2^2\left(l_2^2 + l_1^2 - l_3^2\right) \times \sin(\theta + \phi) + 2ab\cos(\theta)\sin(\phi)\left(l_3^2 l_2^2 - A^2\right) = 0, \tag{43}$$

for which a solution may be most conveniently found graphically, while asymptotic transitions occur when:

$$\theta = \tan^{-1}\left(-\frac{2ab\sin(\phi)}{a^2 - b^2}\right). \tag{44}$$

[4] Note that a continuous transition in for ν_{21} corresponds to a discontinuous transition for ν_{12} and *vice versa*.

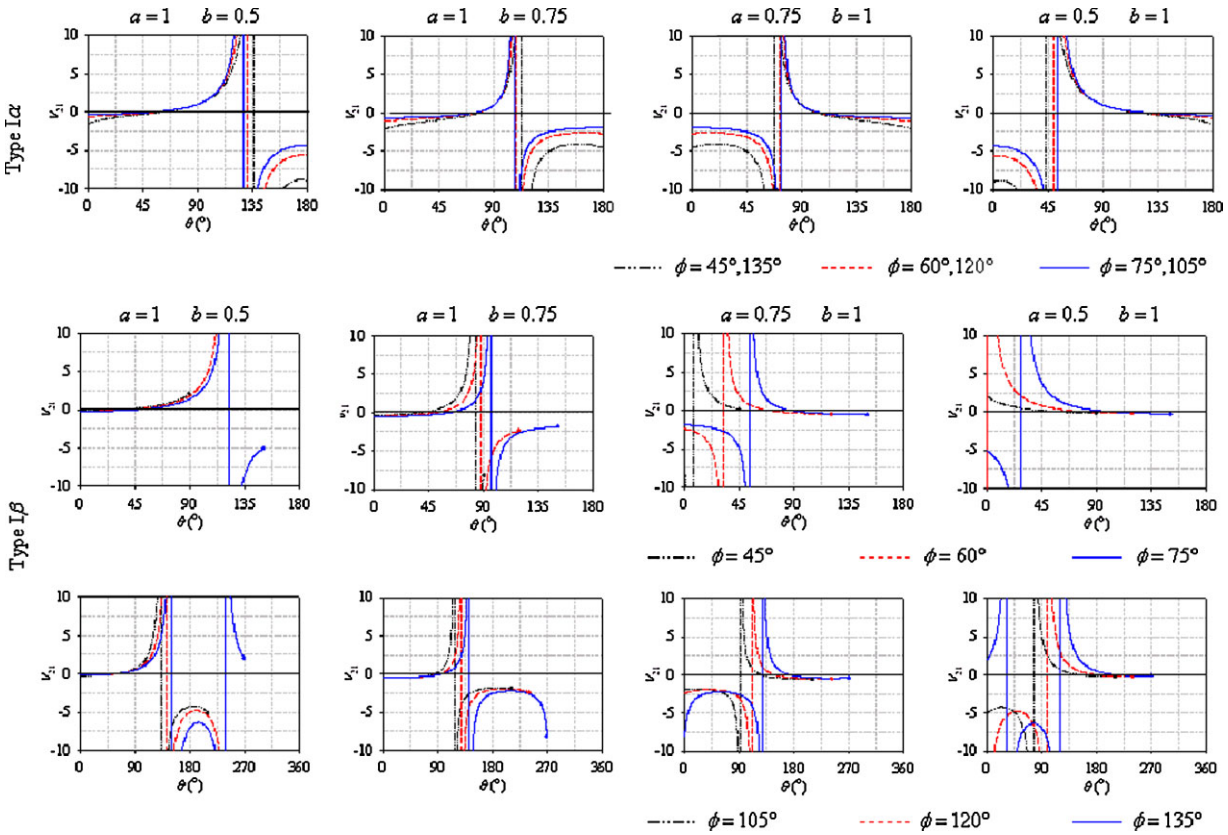

Figure 4 (online colour at: www.pss-b.com) Plots showing the variation of the Poisson's ratio ν_{21} for the Type Iα and Type Iβ parallelograms as they are stretched from their fully closed to their fully open configuration. Note that in the case of the Type Iβ, the filled circles at the end of the lines indicate the limiting value of $\theta = 2\phi$ necessary to avoid overlap of the parallelograms.

Also of interest for Type Iα networks are cases when $\theta = \pi/2$ (except those for which $a = b$). These correspond to instances when the pores are fully open and with a square shape so that the unit cell is also a square, *i.e.* $l_1 = l_2 = l$ and $l_3 = \sqrt{2}l$ at which point $\nu_{21} = 1$ irrespective of the shape and size of the parallelograms.

In the case of Type Iβ, transitions from negative to positive values (or *vice versa*) for ν_{21} are continuous when:

$$\theta = 2\tan^{-1}\left(\frac{\sin(\phi)}{a/b + \cos(\phi)}\right) \text{ or}$$

$$\theta = 2\tan^{-1}\left(\frac{\sin(\phi)}{\cos(\phi) - a/b}\right), \tag{45}$$

and discontinuous when:

$$\theta = 2\tan^{-1}\left(\frac{a/b - \cos(\phi)}{\sin(\phi)}\right) \text{ or}$$

$$\theta = 2\tan^{-1} -\left(\frac{a/b + \cos(\phi)}{\sin(\phi)}\right), \tag{46}$$

whichever condition occurs first and providing that $0<\theta<2\phi$ in order to avoid overlap of the parallelograms themselves. This suggests that a maximum of four transitions, two continuous and two asymptotic, can occur while stretching the system from a fully closed to a fully open configuration, the number of which ultimately depends on ϕ.

In cases where $\phi = \pi/2$, the networks described here, both become equivalent to Type I rectangles with a Poisson's ratio (see Fig. 5b) given by:

$$\nu_{21} = (\nu_{12})^{-1} = \frac{a^2\sin^2\left(\frac{\theta}{2}\right) - b^2\cos^2\left(\frac{\theta}{2}\right)}{a^2\cos^2\left(\frac{\theta}{2}\right) - b^2\sin^2\left(\frac{\theta}{2}\right)}, \tag{47}$$

which has already been discussed in Ref. [26]. For networks which in addition to having $\phi = \pi/2$ also have $a = b$, the Poisson's ratio simplifies further to -1 (Fig. 5c), corresponding to that of the rotating squares [23].

Also interesting are special cases where $a = b$ (Fig. 5a) when $\phi \neq \pi/2$ *i.e.* when the parallelograms become rhombi (but not squares). In these cases we only have two possible networks, the Type α and Type β as described in Ref. [29] where it was shown that the Type β rotating rhombi exhibit constant Poisson's ratio of -1, a property which

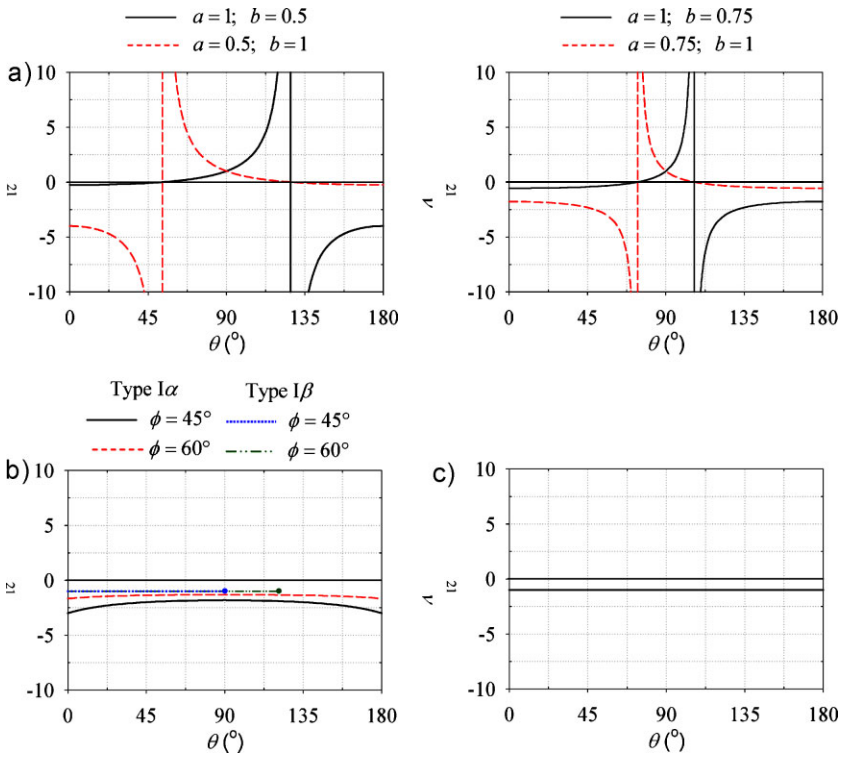

Figure 5 (online colour at: www.pss-b.com) Plots showing the variation of the Poisson's ratio with the degree of openness of the systems for cases where (a) $\phi = 90^\circ$, (b) $a/b = 1$ and (c) $\phi = 90^\circ$ and $a/b = 1$.

is also shown by all Type IIβ parallelograms and by Eq. (30) in the special case $a = b$ (*i.e.* when the Type Iβ parallelograms become Type β rhombi). We also note that the expression for the on-axis Poisson's ratio derived for Orientation 2 reduces to the one derived in [28] when $a = b$ whilst using Eq. (13), it can be shown that the Poisson's ratio for Type α rhombi in Orientation 1 is given by

$$\nu_{21} = -\frac{l_2^2\left(2l_2^2 - l_3\right)\sin(\theta+\phi) + \cos(\theta)\sin(\phi)\left(l_3^2 l_2^2 - A^2\right)}{\cos(\theta)\sin(\phi)\,A^2}. \tag{48}$$

Before we conclude we note that the equations derived in this paper once again show that the Poisson's ratio of the different structures discussed here is scale independent although in general it is dependent on the shape of the parallelograms, the way they are connected, the angle between them and the direction of loading. This suggests that these 'connected parallelograms' may be implemented at any scale and thus may be useful to experimentalists who may inspire themselves from them when they are making real systems at any scale which could mimic the ones described here. In particular, the real systems could be designed in such a way that one or more of the projections of the 3D structure is describable by connected parallelograms, *i.e.* in a similar way that the (001) plane of the zeolite NAT may be described in terms of 'connected squares'. In such cases, the expression derived here will be of particular use to experimentalists as they can help them design systems which exhibit tailor made properties. In this respect we wish to highlight the differences which arise through changing the mode of connectivity.

Finally, it is important to note that whilst it is fairly easy to construct 2D macrostructures with these connectivities where the parallelograms remain rigid, if these system had to be implemented at the micro or nanoscale, one is likely to find that the parallelogrammic units will not be perfectly rigid and instead deform to some extent or another. In such cases, the extent of agreement between the expressions derived here and the properties observed in the real systems will depend on the extent of rigidity of the parallelogrammic units.

6 Conclusion In this work we have derived and discussed the in-plane mechanical properties for Type Iα, Iβ and IIβ parallelograms which together with the Type IIα provide us with a complete picture of all the four different systems that may be constructed from connected parallelograms. We found that these four systems have very different properties from each other with the Type IIβ systems exhibiting constant Poisson's ratios of -1 whilst all other systems have Poisson's ratios which depend on the shape of the parallelograms, the degree of openness and the direction of loading. We also showed that these systems exhibit very different shear behaviour from each other. We hope that this work will help experimentalists in their quest for manufacturing real auxetic systems as the models can assist them in their design of system which can have tailor-made mechanical properties.

Acknowledgements We gratefully acknowledge the financial support of the Malta Council for Science and Technology through the National RTDI programme and of the Malta Government Scholarship Scheme (Grant Number ME 367/07/17 awarded to Daphne Attard).

Appendix A: Mechanical properties of Type Iα and Type Iβ parallelograms in Orientation 2

A1. Type Iα rotating parallelograms The mechanical properties for Type Iα systems in Orientation 2 can be derived using a method very similar to that of Orientation 1 except that for Orientation 2, referring to Fig. 6a, l_1, l_2 and l_3 are given by

$$l_1 = \sqrt{a^2 + b^2 - 2ab\cos(\phi + \theta)}, \tag{49}$$

$$l_2 = \sqrt{a^2 + b^2 + 2ab\cos(\phi - \theta)}, \tag{50}$$

$$l_3 = 2\sqrt{a^2\sin^2\left(\frac{\theta}{2}\right) + b^2\cos^2\left(\frac{\theta}{2}\right) + ab\sin(\theta)\sin(\phi)}. \tag{51}$$

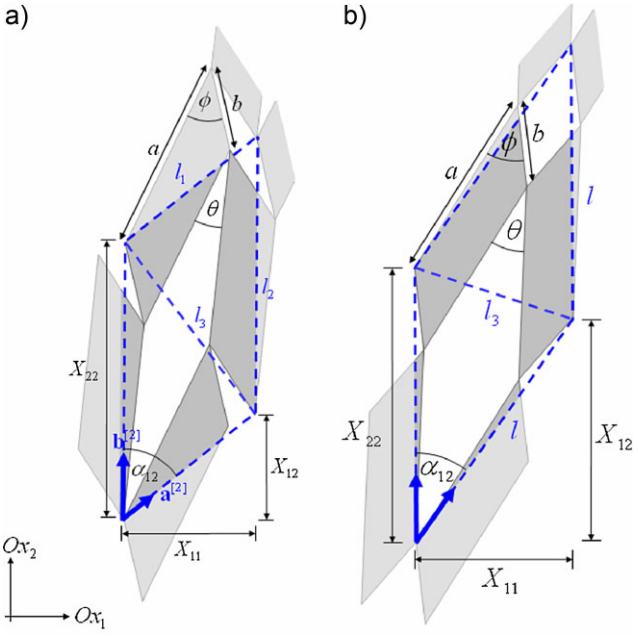

Figure 6 (online colour at: www.pss-b.com) Geometrical parameters describing the unit cell for (a) Type Iα and (b) Type Iβ rotating parallelograms in Orientation 2.

The strains along the Ox_1 and Ox_2 directions can be expressed using Eqs. (11) and (12) so that the Poisson's ratio ν_{21} can be written as

$$\nu_{21} = (\nu_{12})^{-1} = -\frac{\varepsilon_1}{\varepsilon_2} = -\frac{abl_2^4\sin(\theta+\phi) - ab\sin(\phi-\theta)\left(A^2 - l_1^2l_2^2\right) + \frac{1}{2}l_2^2\sin(\theta)\left(a^2-b^2\right)\left(l_1^2+l_2^2-l_3^2\right).}{abA^2\sin(\phi-\theta)} \tag{52}$$

The Young's moduli for Orientation 2 can be found using the same method as for Orientation 1 except that now, in each unit cell there are four hinges rather than eight so that the energy, U stored per unit volume, V is given by

$$U = \frac{2K_h d\theta^2}{V} = \frac{1}{2}E_i\varepsilon_i^2, \tag{53}$$

where $V = X_{11}X_{22}z$, with z being the out-of-plane thickness of the parallelograms so that the Young's moduli can be given by

$$E_1 = \frac{4K_hA^3}{z\left(l_2^2ab\sin(\phi+\theta) - ab\left(\frac{A^2}{l_2^2} - l_1^2\right)\sin(\phi-\theta) + \frac{1}{2}(a^2-b^2)\sin(\theta)\left(l_1^2+l_2^2-l_3^2\right)\right)^2}, \tag{54}$$

$$E_2 = \frac{4K_hl_2^4}{za^2b^2A\sin^2(\phi-\theta)}. \tag{55}$$

In this Orientation Type Iα networks also shear. Using Eq. (18), the shear strain γ can be written as

$$\gamma = \frac{ab\sin(\phi-\theta)\left(l_1^2+l_2^2-l_3^2\right) + l_2^2\left(a^2-b^2\right)\sin(\theta)}{l_2^2A}d\theta, \tag{56}$$

while the shear modulus itself is given by

$$G_{12} = \frac{2U}{\gamma^2} = \frac{4K_hd\theta^2}{V\gamma^2} = \frac{4K_hl_2^4A}{z\left(ab\left(l_1^2+l_2^2-l_3^2\right)\sin(\phi-\theta) + l_2^2(a^2-b^2)\sin(\theta)\right)^2}, \tag{57}$$

and the stiffness coupling coefficients η_{13}, η_{31}, η_{23} and η_{32} are given by

$$\eta_{13} = (\eta_{31})^{-1} = \frac{\gamma}{\varepsilon_1}$$
$$= \frac{4A\left[l_2^2 \sin(\theta)\left(a^2-b^2\right) + ab\left(l_1^2+l_2^2-l_3^2\right)\sin(\phi-\theta)\right]}{l_2^2\left[\left(l_1^2-l_2^2+l_3^2-\frac{2A^2}{l_2^2}\right)ab\sin(\phi-\theta) + ab\left(l_1^2-l_2^2-l_3^2\right)\sin(\phi+\theta) + \left(l_3^2-l_1^2-l_2^2\right)\left(\left(a^2-b^2\right)\sin(\theta)+2ab\cos\theta\sin\phi\right)\right]}\mathbb{S}, \tag{58}$$

$$\eta_{23} = (\eta_{23})^{-1} = \frac{\gamma}{\varepsilon_2}$$
$$= -\frac{l_2^2\left(a^2-b^2\right)\sin(\theta) + ab\left(l_1^2+l_2^2-l_3^2\right)\sin(\phi-\theta)}{abA\sin(\phi-\theta)}. \tag{59}$$

From these equations, it can be shown that when $a = b$, $\alpha_{12} = 90^\circ$ and therefore $A = l_1 l_2$ so that Eq. (52) reduces to

$$\nu_{21} = \frac{\sin(\phi+\theta)(1+\cos(\phi-\theta))}{\sin(\phi-\theta)(\cos(\phi+\theta)-1)}$$
$$= \tan\left(\frac{\theta-\phi}{2}\right)\tan\left(\frac{\theta+\phi}{2}\right), \tag{60}$$

while γ becomes zero, which is equivalent to that for the rotating rhombi in orientation 2 [32].

A2. Type Iβ rotating parallelograms For Type Iβ networks, the unit cell in Orientation 2, shown in Fig 6b, is rhombic rather than rectangular as in Orientation 1, and can be described by the unit-cell vectors $\boldsymbol{a} = (X_{11}, X_{12})$ and $\boldsymbol{b} = (X_{22}, 0)$, given by the following equations:

$$X_{11} = l\sin(\alpha_{12}), \tag{61}$$

$$X_{22} = l, \tag{62}$$

$$X_{12} = l\cos(\alpha_{12}), \tag{63}$$

where

$$l = \sqrt{a^2+b^2+2ab\cos(\theta-\phi)}, \tag{64}$$

$$\sin(\alpha_{12}) = \frac{{X_{11}}^{[1]}{X_{22}}^{[1]}}{2l^2};\quad \cos(\alpha_{12}) = 1-\frac{1}{2}\left(\frac{{X_{22}}^{[1]}}{l}\right)^2, \tag{65}$$

with $X_{11}^{[1]}$ and $X_{22}^{[1]}$ being the unit cell dimensions along the Ox_1 and Ox_2 directions respectively for Orientation 1 so that after substituting for these terms using Eqs. (24) and (25), the strains can be found by differentiating X_{11} and X_{22} with respect to θ as follows:

$$\varepsilon_1 = \frac{a^2\cos(\theta) - b^2\cos(2\phi-\theta) - ab\sin(\alpha_{12})\sin(\phi-\theta)}{l^2\sin(\alpha_{12})}\mathrm{d}\theta, \tag{66}$$

$$\varepsilon_2 = \frac{ab\sin(\phi-\theta)}{l^2}\mathrm{d}\theta, \tag{67}$$

so that the Poisson's ratio is then given by

$$\nu_{21} = 1-\frac{l^2\left[a^2\cos(\theta) - b^2\cos(2\phi-\theta)\right]}{ab\sin(\phi-\theta)\left[a^2\sin(\theta)+2ab\sin(\phi)+b^2\sin(2\phi-\theta)\right]}, \tag{68}$$

which becomes -1 for cases where $a = b$, *i.e.* when the parallelograms become rhombi [32].

Also, using Eq. (53), the Young's moduli are given by

$$E_1 = \frac{4K_h l^2\sin(\alpha_{12})}{z\left(a^2\cos(\theta) - b^2\cos(2\phi-\theta) - ab\sin(\alpha_{12})\sin(\phi-\theta)\right)^2}, \tag{69}$$

$$E_2 = \frac{4K_h l^2}{z\sin(\alpha_{12})\left(ab\sin(\phi-\theta)\right)^2}. \tag{70}$$

As opposed to Orientation 1, in Orientation 2, these networks also shear. The shear strain can be found using Eq. (18), putting $l_1 = l_2 = l$ so that after simplifying, the shear strain γ is given by

$$\gamma = -\frac{a^2\cos(\theta) - b^2\cos(2\phi-\theta) - 2ab\sin(\alpha_{12})\sin(\phi-\theta)}{abl^2\cos(\alpha_{12})\sin(\phi-\theta)}\mathrm{d}\theta, \tag{71}$$

so that using an energy approach, the shear modulus is given by

$$G_{12} = \frac{4K_h \mathrm{d}\theta^2}{V\gamma^2} = \frac{4K_h l^2 \cos^2(\alpha_{12})}{z \sin(\alpha_{12}) \left[a^2 \cos(\theta) - b^2 \cos(2\phi - \theta) - 2ab \sin(\alpha_{12}) \sin(\phi - \theta)\right]^2}, \tag{72}$$

while the shear coupling coefficients are given by

$$\eta_{13} = (\eta_{31})^{-1} = \frac{\sin(\alpha_{12}) \left[a^2 \cos(\theta) - b^2 \cos(2\phi - \theta) - 2ab \sin(\alpha_{12}) \sin(\phi - \theta)\right]}{\cos(\alpha_{12}) \left[a^2 \cos(\theta) - b^2 \cos(2\phi - \theta) - ab \sin(\alpha_{12}) \sin(\phi - \theta)\right]}, \tag{73}$$

$$\eta_{23} = (\eta_{23})^{-1} = \frac{a^2 \cos(\theta) + b^2 (2\phi - \theta) - 2ab \sin(\alpha_{12}) \sin(\phi - \theta)}{ab \cos(\alpha_{12}) \sin(\phi - \theta)}. \tag{74}$$

References

[1] A. Alderson, Chemistry and Industry 384 (1999) available online at http://web.mit.edu/course/3/3.91/OldFiles/www/slides/Auxetic_Foams.pdf.
[2] R. S. Lakes and K. Elms, J. Compos. Mater. **27**, 1193 (1993).
[3] K. E. Evans and A. Alderson, Adv. Mater. **12**, 617 (2000).
[4] K. E. Evans, M. A. Nkansah, I. J. Hutchinson, and S. C. Rogers, Nature **353**, 124 (1991).
[5] R. Lakes, Science **235**, 1038 (1987).
[6] K. E. Evans and A. Alderson, Adv. Mater. **12**, 617 (2000).
[7] F. Scarpa, L. G. Ciffo, and J. R. Yates, Smart Mater. Struct. **13**, 49 (2004).
[8] F. Scarpa and F. C. Smith, J. Intel. Mat. Syst. Str. **15**, 973 (2004).
[9] F. Scarpa, W. A. Bullough, and P. Lumley, P. I. Mech. Eng. C - J. Mech. Eng. Sci. **218**, 241 (2004).
[10] K. W. Wojciechowski, Mol. Phys. **61**, 1247 (1987).
[11] K. W. Wojciechowski and A. C. Branka, Phys. Rev. A **40**, 7222 (1989).
[12] K. W. Wojciechowski, J. Phys. A – Mat. Gen. **36**, 11765 (2003).
[13] J. W. Narojczyk, A. Alderson, A. R. Imre, F. Scarpa, and K. W. Wojciechowski, J. Non-Cryst. Solids **354**, 4242 (2008).
[14] K. V. Tretiakov and K. W. Wojciechowski, Phys. Status Solidi B **242**, 730 (2005).
[15] K. V. Tretiakov and K. W. Wojciechowski, Phys. Status Solidi B **244**, 1038 (2007).
[16] M. Bowick, A. Cacciuto, G. Thorleifsson, and A. Travesset, Phys. Rev. Lett. **87**, 148103 (2001).
[17] F. K. Abd El-Sayed, R. Jones, and I. W. Burgens, Composites **10**, 209 (1979).
[18] L. J. Gibson, M. F. Ashby, G. S. Schajer, and C. I. Robertson, Proc. R. Soc. Lond. A **382**, 25 (1982).
[19] I. G. Masters and K. E. Evans, Compos. Struct. **35**, 403 (1996).
[20] K. E. Evans, A. Alderson, and F. R. Christian, J. Chem. Soc. Faraday T. **91**, 2671 (1995).
[21] D. Prall and R. S. Lakes, Int. J. Mech. Sci. **39**, 305 (1997).
[22] A. Spadoni, M. Ruzzene, and F. Scarpa, Phys. Status Solidi B **242**, 695 (2005).
[23] J. N. Grima and K. E. Evans, J. Mater. Sci. Lett. **19**, 1563 (2000).
[24] Y. Ishibashi and M. Iwata, J. Phys. Soc. Jpn. **69**, 2702 (2000).
[25] J. N. Grima, R. Gatt, A. Alderson, and K. E. Evans, J. Phys. Soc. Jpn. **74**, 2866 (2005).
[26] J. N. Grima, A. Alderson, and K. E. Evans, Phys. Status Solidi B **242**, 561 (2005).
[27] J. N. Grima and K. E. Evans, J. Mater. Sci. **41**, 3193 (2006).
[28] J. N. Grima, P. S. Farrugia, R. Gatt, and D. Attard, Phys. Status Solidi B **245**, 521 (2008).
[29] D. Attard and J. N. Grima, Phys. Status Solidi B **245**, 2395 (2008).
[30] J. N. Grima, V. Zammit, R. Gatt, A. Alderson, and K. E. Evans, Phys. Status Solidi B **244**, 866 (2007).
[31] A. Alderson and K. E. Evans, Phys. Chem. Miner. **28**, 711 (2001).
[32] A. Alderson and K. E. Evans, Phys. Rev. Lett. **89**, 10.1103. (2002).
[33] A. Alderson, K. L. Alderson, K. E. Evans, J. N. Grima, M. R. Williams, and P. J. Davies, Comput. Methods Sci. Technol. **10**, 117 (2004).
[34] A. Alderson, K. L. Alderson, K. E. Evans, M. R. Williams, and P. J. Davies, Phys. Status Solidi B **242**, 499 (2005).
[35] R. F. Almgren, J. Elast. **15**, 427 (1985).
[36] J. N. Grima, New Auxetic Materials, PhD Thesis, University of Exeter, Exeter, UK 2000.
[37] A. Alderson, P. J. Davies, M. R. Williams, K. E. Evans, K. L. Alderson, and J. N. Grima, Mol. Simul. **31**, 897 (2005).
[38] J. N. Grima, J. J. Williams, R. Gatt, and K. E. Evans, Mol. Simul. **31**, 907 (2005).
[39] J. N. Grima, D. Attard, R. Cassar, L. Farrugia, L. Trapani, and R. Gatt, Mol. Simul. **34**, 1149 (2008).
[40] J. N. Grima and K. E. Evans, Chem. Commun. **16**, 1531 (2000).

[41] J. N. Grima, J. J. Williams, and K. E. Evans, Chem. Commun. **4065**, (2005).
[42] G. Wei, Phys. Status Solidi B **242**, 742 (2005).
[43] J. N. Grima, A. Alderson, and K. E. Evans, J. Phys. Soc. Jpn. **74**, 1341 (2005).
[44] C. W. Smith, J. N. Grima, and K. E. Evans, Acta Mater. **48**, 4349 (2000).
[45] N. Gaspar, X. J. Ren, C. W. Smith, J. N. Grima, and K. E. Evans, Acta Mater. **53**, 2439 (2005).
[46] J. N. Grima, R. Gatt, N. Ravirala, A. Alderson, and K. E. Evans, Mater. Sci. Eng. A **423**, 214 (2006).
[47] K. E. Evans, M. A. Nkansah, and I. J. Hutchinson, Acta Metall. Mater. **42**, 1289 (1994).
[48] B. D. Caddock and K. E. Evans, J. Phys. D: Appl. Phys. **22**, 1877 (1989).
[49] K. L. Alderson and K. E. Evans, J. Mater. Sci. **28**, 4092 (1993).
[50] A. P. Pickles, K. L. Alderson, and K. E. Evans, Polym. Eng. Sci. **36**, 636 (1996).
[51] J. N. Grima, R. Gatt, A. Alderson, and K. E. Evans, Mater. Sci. Eng. A **423**, 219 (2006).
[52] J. N. Grima, R. Gatt, A. Alderson, and K. E. Evans, J. Mater. Chem. **15**, 4003 (2005).
[53] R. H. Baughman, J. M. Shacklette, A. A. Zakhidov, and S. Stafstrom, Nature **392**, 362 (1998).
[54] C. He, P. Liu, and A. C. Griffin, Macromolecules **31**, 3145 (1998).
[55] C. He, P. Liu, P. J. McMullan, and A. C. Griffin, Phys. Status Solidi B **242**, 576 (2005).
[56] J. N. Grima, R. Jackson, A. Anderson, and K. E. Evans, Adv. Mater. **12**, 1912 (2000).
[57] J. N. Grima, P. S. Farrugia, C. Caruana, R. Gatt, and D. Attard, J. Mater. Sci. **43**, 5962 (2008).
[58] J. N. Grima, P. S. Farrugia, R. Gatt, and V. Zammit, Proc. R. Soc. Lond. A **463**, 1585 (2007).
[59] J. F. Nye, Physical Properties of Crystals (Clarendon Press, Oxford, 1957).

